RSC Advances

This article can be cited before page numbers have been issued, to do this please use: M. Govindasamy, S. Chen, V. mani, A. Sathiyan, P. Merlin, A. Fahad M.A. and A. Ali, *RSC Adv.*, 2016, DOI: 10.1039/C6RA18740D.

ROYAL SOCIETY OF CHEMISTRY

www.rsc.org/advances

View Article Online
DOI: 10.1039/C6RA18740D

Simultaneous determination of dopamine and uric acid in presence of high concentration of ascorbic acid using cetyltrimethylammonium bromide–polyaniline/activated charcoal composite

Mani Govindasamy[1], Shen-Ming Chen[1], Veerappan Mani[1,2]*, Anandaraj Sathiyan[3], Johnson Princy Merlin[3], Fahad M.A. Al-Hemaid[4], M. Ajmal Ali[4]*

[1]Department of Chemical Engineering and Biotechnology, National Taipei University of Technology, Taipei, Taiwan (ROC)

[2]Graduate Institute of Biomedical and Biochemical Engineering, National Taipei University of Technology, Taipei, Taiwan (ROC)

[3]Department of Chemistry, Bishop Heber College (Autonomous), Tiruchirappalli-620 017, Tamil Nadu, India

[4]Department of Botany and Microbiology, College of Science, King Saud University, Riyadh 11451, Saudi Arabia

Corresponding author: V. Mani, Email: veera.678@gmail.com Tel.: +886 2271-2171 2525; Fax: +886-02-2731-7117. S.-M. Chen, Email: smchen78@ms15.hinet.net Tel: +886 2270 17147, Fax: +886 2270 25238

View Article Online
DOI: 10.1039/C6RA18740D

Abstract

We described a simple, low-cost and mass producible composite made up of cetyltrimethylammonium bromide (CTAB) functionalized polyaniline (PANI) and activated charcoal (CTAB–PANI/AC) for simultaneous determination of dopamine (DA) and uric acid (UA). The composite formation was verified through scanning electron microscopy, electrochemical impedance spectroscopy and electrochemical methods. The CTAB–PANI/AC composite was used to modify glassy carbon electrode (GCE) and the resulting modified electrode displayed excellent electrocatalytic activity to DA and UA and successfully separates their overlapped voltammetric peaks. The composite completely inhibits the AA signal and does not produce any voltammetric signal for AA upto 2 mM. The DA and UA can be selectively detectable upto detection limits of 0.06 (± 0.006) μM and 0.20 (± 0.008) μM, respectively. The effect of kinetics, analyte concentrations and pH of the supporting electrolyte pH investigated and optimized. The modified electrode has appreciable stability, repeatability and reproducibility. Besides, practical feasibility of the sensor is demonstrated in biological samples which delivered satisfactory recovery results.

Keywords: Activated carbon materials, analytical science, conducting polymers, electrocatalysis, electrochemical sensors, bioassays, neurotransmitters

1. Introduction

Dopamine (DA) is one of the key neurotransmitter in mammalian central nervous systems which facilities communication between brain and neurons.[1-3] Abnormal concentration of DA is directly related to motor functions of the central nervous system which can cause several neurological disorders.[4, 5] In addition, DA is administered externally as a medication to DA deficient patients, but its excess dosage causes neurological side effects.[6] Therefore, sensitive determination of DA is important in clinical analysis.[7-9] Besides, uric acid (UA) is the primary end product of purine metabolism and its abnormal levels are symptoms of several diseases such as gout, hyperuricemia and Lesch-Nyan disease.[10, 11] It is well-known that DA, UA and ascorbic acid (AA) are usually coexisted in the extra cellular fluids; however, they are indicators for different diseases.[12, 13] AA is a significant vitamin required for human diet and

View Article Online
DOI: 10.1039/C6RA18740D

usually its concentration in extra cellular fluids is much higher (about 1000 times) than that of DA and UA. Hence, the detections of DA and UA always encountered strong interference from AA.[14, 15] In addition, the electrode surface is susceptible to get damaged by the adsorption of oxidized products of AA which leads to surface fouling and film stability problems.[16] The other problems in the determinations of DA and UA are overlapped voltammetric responses, poor selectivity and low reproducibility.[17] The bare electrodes are not suitable for either selective and/or simultaneous detections of DA and UA and hence rationally designed chemical modifiers are required.[18] The ideal modifiers should separate the voltammetric peaks of DA and UA with wide peak-to-peak separation, completely eliminate the AA interference, high sensitivity in presence of AA, and selectivity over coexisted electroactive species in biological fluids. So far, several modified electrodes based on nanomaterials [7, 17], conducting polymers [1, 19], metal nanoparticles [7, 20] and metal oxides [21, 22] were developed; however not all of them are ideal modifiers.[23] Xu et al., have reported Pt nanoparticles supported reduced graphene oxide for the simultaneous detection of DA and UA which eliminates AA interference upto 1 mM.[14] Liu et al., described poly(acrylic acid)-multiwalled carbon nanotubes composite for the detections of DA and UA which hinders AA signal upto 0.3 mM.[24] Alipour et al., described pretreated pencil graphite electrode for the detections of DA and UA which is selective upto 0.5 mM AA.[17] In spite of the success of developed electrode materials, new materials are still in demand to completely tackle the problems due to the biological significance of DA and UA.

Polyaniline (PANI) is the most popularly used conducting polymer in electrochemical sensors attributed to its excellent electrocatalytic ability, conductivity, easy synthesis, high environmental stability and thermal stability.[25] The composites of PANI with carbon materials such as, activated carbon, graphene and carbon nanotubes have shown improved electronic and mechanical properties compared with pure PANI, making the composite more suitable for electronic/electrochemical applications.[26] Among other carbon materials, activated carbon/charcoal (AC) is the cheapest, most abundant and it possesses high surface area and good porosity[27]. In recent times, the composite prepared from AC and PANI is attracted significant attention in supercapacitors.[27-29] Nevertheless, the electrochemical sensor applicability of AC/PANI composite is not investigated in the literature.

View Article Online
DOI: 10.1039/C6RA18740D

Herein, we have prepared AC/PANI composite via simple soft-template synthetical method using CTAB as template and explored its electrochemical sensing applicability towards simultaneous determinations of DA and UA. Previous studies proved that CTAB is a good soft-template for controlled polymerization of aniline and the resulting polymer is ordered in different aspects, such as morphology, particle size, and conductivity[30], while we have used potassium peroxodisulfate (PDS) as a radical initiator in PANI formation. The positively charged PANI surface is easy to bind with negatively charged AC surface via electrostatic interaction which resulting in the formation of stable composite. The morphology, elemental composition, electrode-electrolyte interface and electrochemical properties are revealing that the CTAB–PANI/AC composite is highly suitable for electrochemical sensing applications. The electrochemical studies proved that the composite is highly useful for simultaneous determination of DA and UA in presence of high concentrations of AA (upto 2 mM) (**scheme 1**).

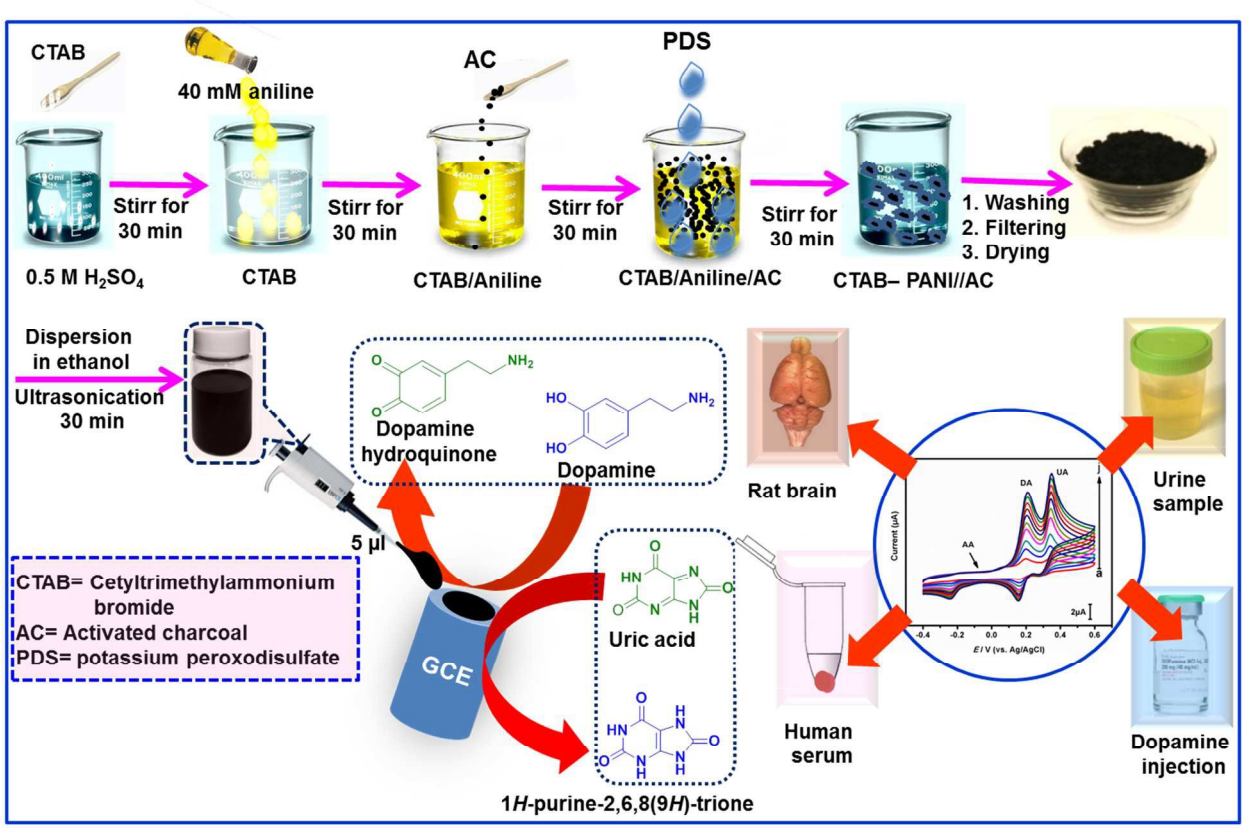

Scheme 1 Schematic representation for the preparation of CTAB–PANI/AC/GCE and its application towards simultaneous determinations of DA and UA

View Article Online
DOI: 10.1039/C6RA18740D

2. Experimental

2.1 Chemicals and Apparatus

Aniline, CTAB, AC and PDS were purchased from Merck. All the other reagents were purchased from Sigma-Aldrich and used as received. All the reagents used were of analytical grade and used without any further purification. Double distilled water was used for all the experiments. 0.1 M phosphate buffer (pH 7.0) was used as supporting electrolyte which was prepared from sodium dihydrogen phosphate and disodium hydrogen phosphate. Rat brain sample and human serum were acquired from Chang Gung University, Taiwan and the experimental protocols were approved by the institutional Animal Ethic Committee. The real sample analysis performed in rat brain and human serum samples were performed in compliance with the laws and institutional guidelines of Chang Gung University, Taiwan. An informed consent was obtained for human serum collection with human subject.

Electrochemical studies were performed in a conventional three electrode cell using modified glassy carbon electrode (GCE) (Bioanalytical Systems, Inc., USA) as a working electrode (area 0.071 cm^2), saturated Ag|AgCl (saturated KCl) as a reference electrode and Pt wire as a counter electrode. All the electrochemical measurements were carried out using CHI 1205a electrochemical work station (CH Instruments, Inc., U.S.A) at ambient temperature. Prior to each electrochemical experiment, the electrolyte solutions were deoxygenated with pre-purified nitrogen for 15 min unless otherwise specified. Surface morphological studies were carried out using Hitachi S-3000 H scanning electron microscope (SEM) and transmission electron microscope (TEM) (H-7600, Hitachi, Japan). Raman spectra were acquired using Micro-Raman spectrometer (RENISHAW in Via system, U.K) by a 514.4 nm He/Ne laser. FTIR spectra were carried out using a Perkin-Elmer IR spectrometer. The X-ray photoelectron spectroscopy was studied by using XPS, PerkinElmer PHI-5702. EIM6ex Zahner (Kronach, Germany) was used for electrochemical impedance spectroscopy (EIS) studies.

2.2 Preparation of CTAB–PANI/AC/GCE

First, 5 mM CTAB solution was prepared in 0.5 M H_2SO_4. Next, 40 mM aniline solution was added to the CTAB solution and the mixture was stirred for 30 min using magnetic stirrer. 1

View Article Online
DOI: 10.1039/C6RA18740D

g of AC was added to the solution and continued stirring for additional 30 min, while the temperature was maintained below 0°C. Afterwards, a pre-cooled solution of 50 mM PDS was added in dropwise to aniline solution and stirred for 30 min. A precipitate was formed which was filtered and washed several times with water and acetone, respectively. The purified CTAB–PANI/AC composite was dried and redispersed in ethanol (1 mg mL^{-1}). Next, GCE surface was polished with 0.05 µm alumina slurry using a Buehler polishing kit, then washed with water and dried. 5 µl dispersion of CTAB–PANI/AC was dropped at the pre-cleaned GCE and dried at ambient conditions.

2.3 Sampling procedure for real sample analysis

Dopamine hydrochloride injection was obtained from local medical hospital and directly used for the analysis. Real-time analysis is directly carried out by injecting aliquots of dopamine hydrochloride injection sample into phosphate buffer (pH 7). In all the real-sample studies, the total volume of the electrochemical cell is kept at 1 mL. Rat brain sample and human serum were acquired from Chang Gung University, Taiwan and the experimental protocols were approved by the institutional Animal Ethic Committee. About 1 mL of rat brain or human serum was added to 20 mL of buffer. To this solution, known concentrations of DA are spiked and analyzed using CTAB–PANI/AC film modified electrode. Human urine sample is collected from a healthy human. About 1 mL of human urine is diluted with 50 mL of phosphate buffer and the resulting solution is DA free. To this solution, known concentrations of DA are spiked and analyzed using our method.[31]

View Article Online
DOI: 10.1039/C6RA18740D

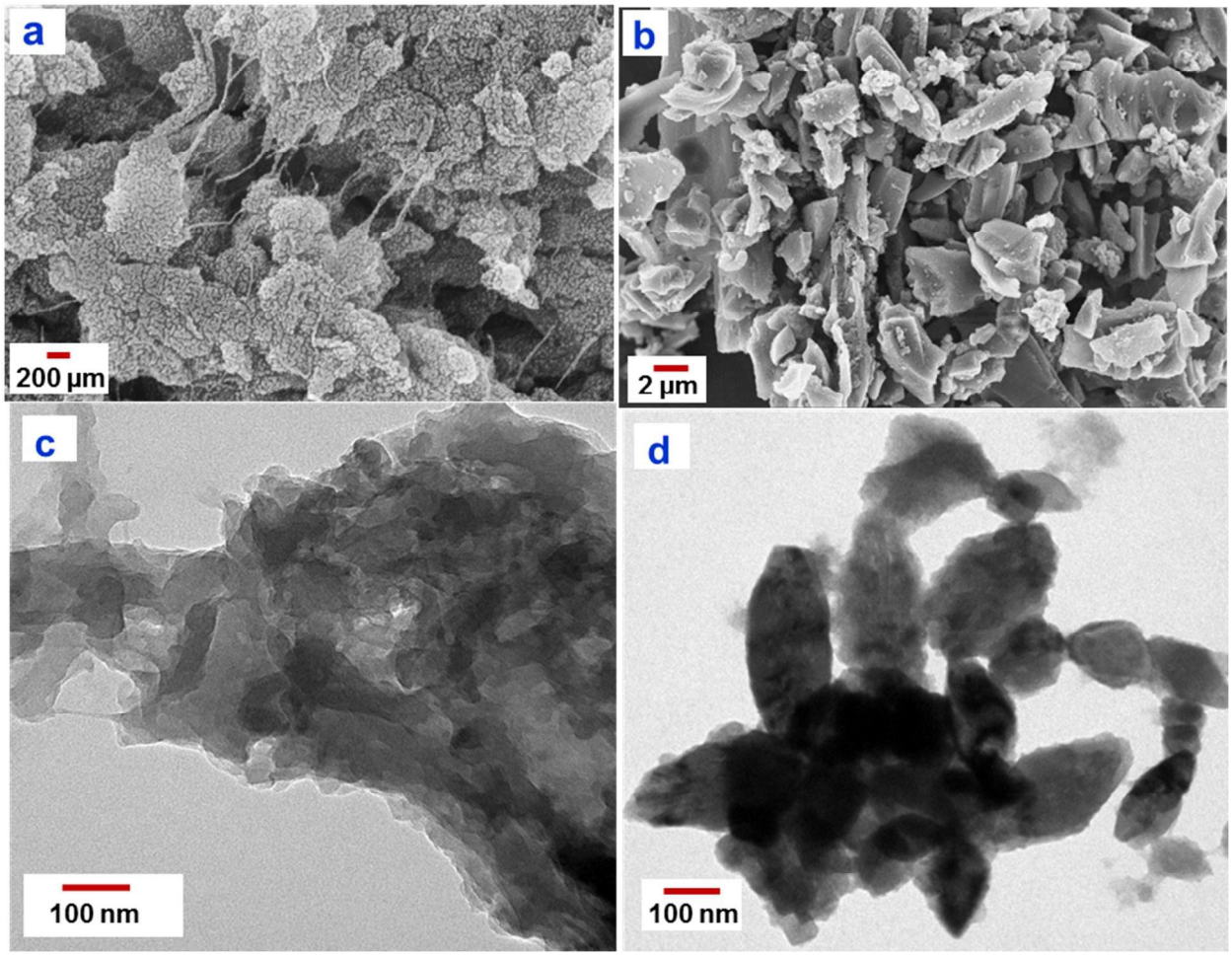

Fig. 1 SEM images of CTAB–PANI (a) and CTAB–PANI/AC composite (b). TEM images of CTAB–PANI (c) and CTAB–PANI/AC composite

View Article Online
DOI: 10.1039/C6RA18740D

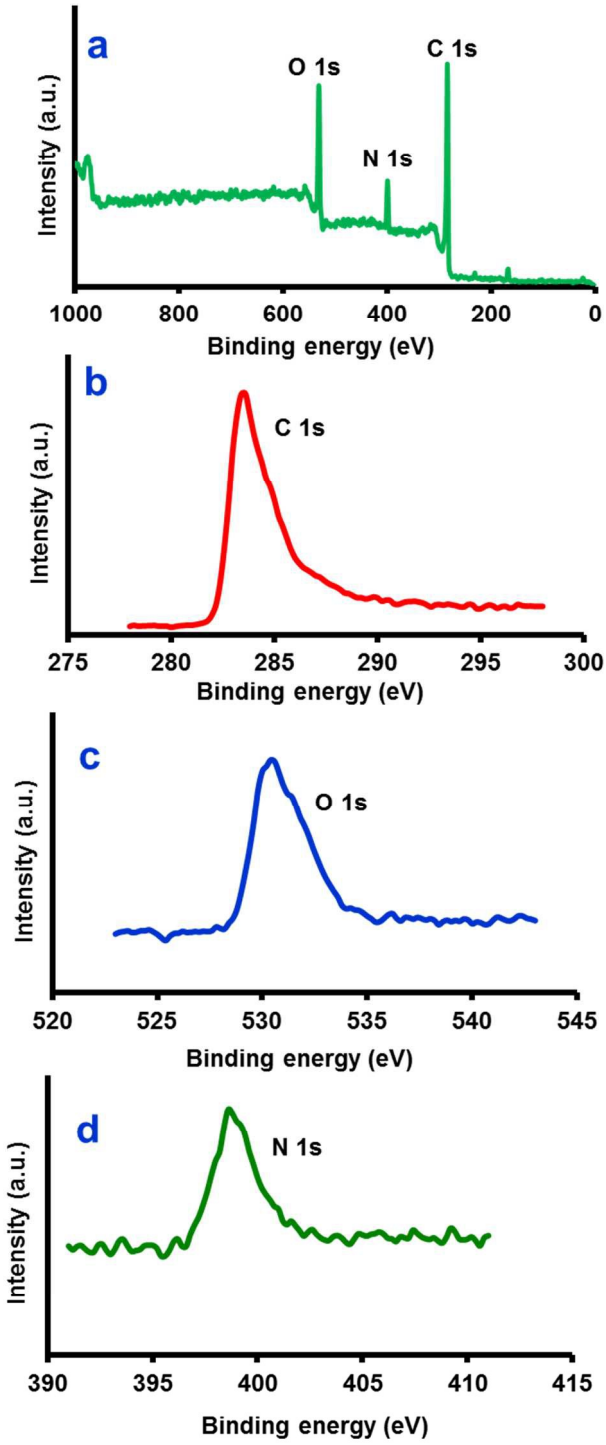

Fig. 2 a) XPS survey spectrum of CTAB–PANI/AC composite. b) C 1s, c) O 1s, d) N 1s,

View Article Online
DOI: 10.1039/C6RA18740D

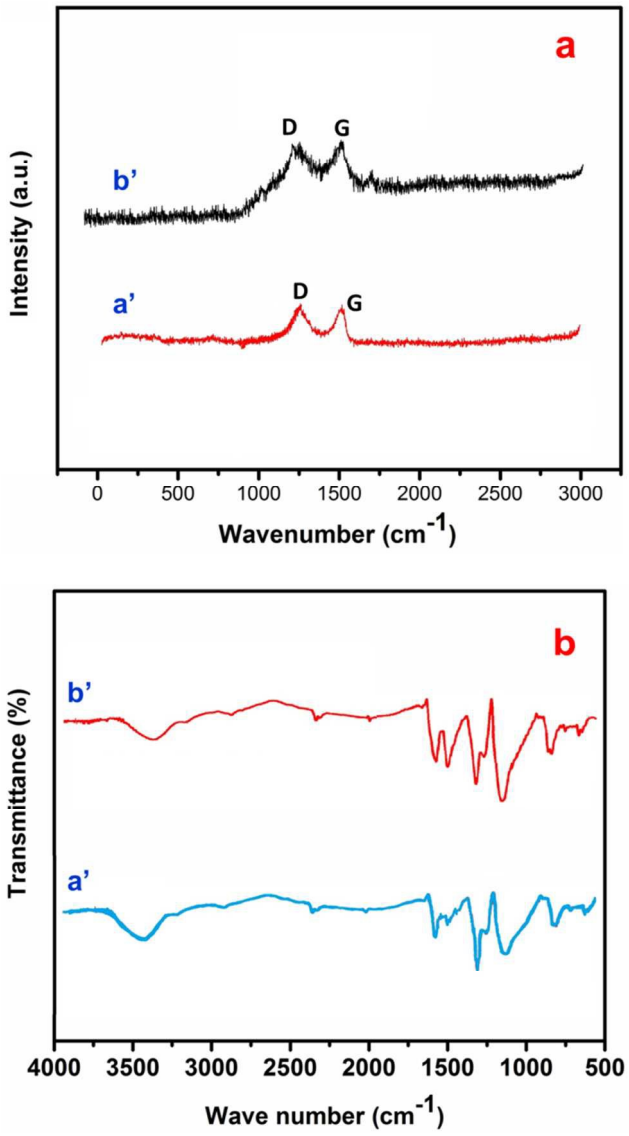

Fig.3 (a) Raman spectra of CTAB–PANI (a') and CTAB–PANI/AC (b'). (b) FT-IR spectra of CTAB–PANI (a') and CTAB–PANI/AC (b')

3. Results and Discussions

3.1 Characterization of CTAB–PANI/AC

The surface morphology of the CTAB–PANI and CTAB–PANI/AC composites were studied using SEM and TEM. The SEM of CTAB–PANI (**Fig. 1a**) exhibited porous like morphology along with the presence of PANI fibers and this kind of morphology is also

View Article Online
DOI: 10.1039/C6RA18740D

observed in the TEM (**Fig. 1c**). The SEM image of CTAB–PANI/AC is featured with highly porous morphology which portrays abundant pores, cavities and randomly distributed flakes (**Fig. 1b**). TEM image of the composite also displays the PANI covered porous carbon like morphology which is consistent with SEM results (**Fig. 1d**). XPS is used to measure the elemental composition of the as-prepared composite (**Fig. 2a**). The survey XPS spectrum indicates that the composite consists of oxygen (O 1s, 532 eV), nitrogen (400 eV) and carbon (C 1s 285 eV). The presence of nitrogen is clearly indicating the successful formation of PANI/AC composite, because the nitrogen content is originated from polyaniline. The enlarged XPS spectra for C1s (**Fig. 3b**), O1s (**Fig. 3c**) and N1s (**Fig. 3d**) are clearly show the typical bands and revealed the successful formation of composite. The Raman spectrum of CTAB-PANI (curve a', **Fig. 4a**) displays two sharp bands at ≈ 1261 cm^{-1} and ≈ 1539 cm^{-1} corresponding to the characteristic D and G bands. Besides, the D band to G band intensity ratio (I_D/I_G) is considerably increased in CTAB–PANI/AC composite (curve b', **Fig. 4a**) and the bands are slightly red shifted compared to CTAB–PANI indicating the possible interaction between CTAB–PANI and AC. FT-IR spectroscopy is used to investigate the functionality of the as-prepared materials. The FTIR spectrum of CTAB–PANI (**curve a', Fig. 4b**) displays FTIR absorption peaks, *ν*(N–H) = 3430, *ν*(aromatic C-H bond)= 2891, *ν*(quinoid)= 1563, *ν*(benzenoid)= 1490, *ν*(C-N stretching and bending vibrations)= 1299 and 1238, *ν*(C-N double bond)= 1115 and *ν*(C-H out of plane bending)= 801 cm^{-1} which are characteristic stretching vibrations of PANI and this result is consistent with previous reports.[32, 33] These vibration modes are observed in CTAB–PANI/AC composite, but slightly red shifted which could be due to the composite formation **(curve b', Fig. 4b**).

View Article Online
DOI: 10.1039/C6RA18740D

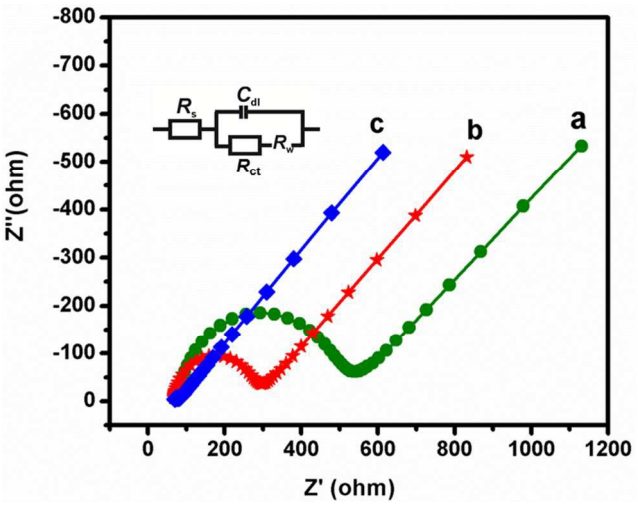

Fig. 4 EIS curves of bare GCE (a), CTAB–PANI (b) and CTAB–PANI/AC composite (c). Inset: Randles equivalent circuit model. Here, R_s is electrolyte resistance, R_{ct} is charge transfer resistance, C_{dl} is double layer capacitance and Z_w is Warburg impedance.

Fig. 4 displays the EIS obtained at bare GCE (a), CTAB–PANI (b) and CTAB–PANI/AC (c) in 0.1 M KCl containing 5 mM $Fe(CN)_6^{3-/4-}$. Randles equivalent circuit model was used to fit the experimental data (**inset to Fig. 4**). The semicircles indicates the parallel combination of electron transfer resistance (R_{ct}) and double layer capacitance (C_{dl}) at electrode surface resulting from electrode impedance. The charge transfer resistance values were obtained by fitting the Nyquist plot results with Randles equivalent circuit model. The R_{ct} values of bare GCE, CTAB–PANI/GCE and CTAB–PANI/AC/GCE are 460 (± 2.18) Ω, 275 (± 3.05) Ω and 25 (± 1.41) Ω respectively. The R_{ct} value obtained at CTAB–PANI/AC/GCE is 11 and 18 times smaller than that of CTAB–PANI/GCE and unmodified GCE, respectively. Thus, CTAB–PANI/AC has lower electrode resistance over control electrodes which are due to the high conductivity and large surface area of the composite.

View Article Online
DOI: 10.1039/C6RA18740D

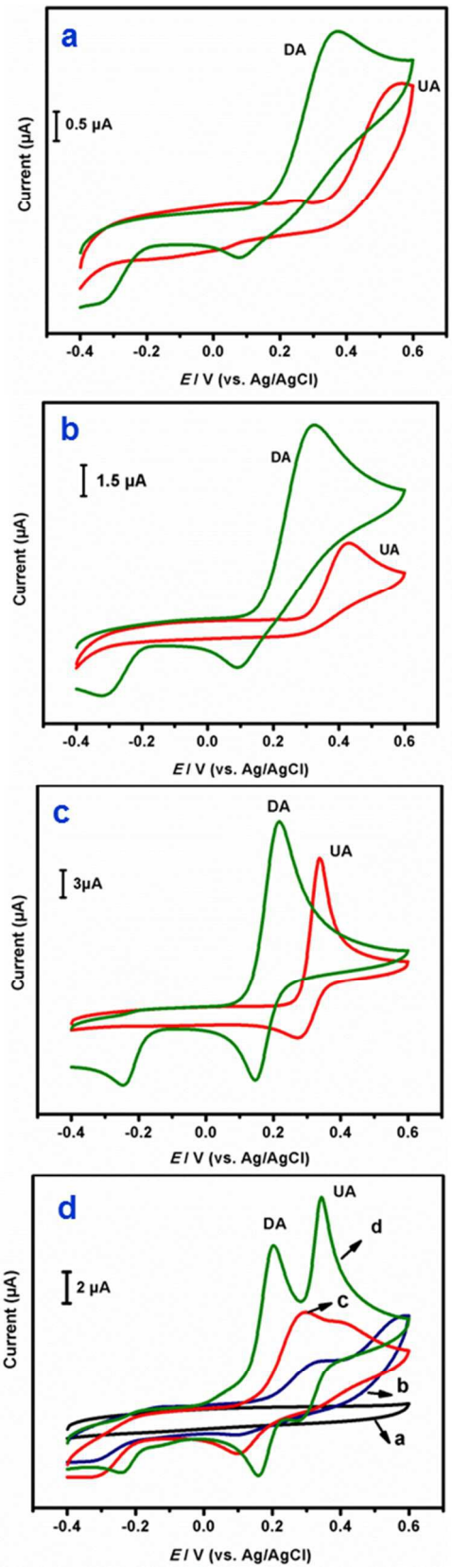

View Article Online
DOI: 10.1039/C6RA18740D

Fig. 5 CVs obtained at bare GCE (a), CTAB–PANI/GCE (b), and CTAB–PANI/AC/GCE (c) in phosphate buffer (pH 7.0) containing 1 mM DA (a) or 0.5 mM UA (b). Scan rate = 50 mV s^{-1}. (d) CVs obtained at bare GCE (b), CTAB–PANI/GCE (c) and CTAB–PANI/AC/GCE (d) in phosphate buffer (pH 7.0) containing mixture of 2 mM DA+2 mM UA. CV of CTAB–PANI/AC/GCE (curve a) in the absence of DA and UA

3.2 Electrocatalysis of DA and UA

Fig.5 shows the cyclic voltammograms (CVs) obtained at unmodified GCE (a), CTAB–PANI/GCE (b), and CTAB–PANI/AC (c) towards 1 mM DA and 0.5 mM UA. The scan rate is 50 mV s^{-1}. Electrochemical parameters for the electrocatalysis of DA and UA such as, anodic (E_{pa}) and cathodic peak potentials (E_{pc}), anodic (i_{pa}) and cathodic peak currents (i_{pc}), and peak potential separation (ΔE_p) at these modified electrodes are given in **Table S1**. The unmodified GCE displays poor electrocatalytic ability to oxidize DA and UA. Although, CTAB–PANI/GCE displays good electrocatalytic ability, the oxidation potentials of DA and UA are closely associated and the oxidation peaks are weak. Comparatively, the CTAB–PANI/AC has shown excellent electrocatalytic ability to DA and UA which is evident from the observation of two sharp and highly enhanced redox peaks. Compared with control electrodes, the CTAB–PANI/AC composite has shown significantly improved electrocatalytic performance due to its large electrochemically accessible surface area. **Fig. 5(d)** displays the CVs of bare GCE (b), CTAB–PANI/GCE (c) and CTAB–PANI/AC/GCE (d) films modified GCEs in phosphate buffer (pH 7.0) containing mixture of 2 mM DA and 2 mM UA. As shown in figure, bare GCE has shown unresolved and weak oxidation peak at 0.30. Although, the CTAB–PANI have showed two oxidation peaks at 0.315 V and 0.40 V, the peak-to-peak separation is not sufficient. Interestingly, CTAB–PANI/AC modified electrode is featured with two strong and well-defined anodic peaks at 0.218 V and 0.335 V, respectively. These peaks are separated by wide peak-to-peak separation gap of about 117 mV, which is fairly enough to perform simultaneous determinations. Hence, CTAB–PANI/AC composite is a qualified hybrid material to perform simultaneous detections of DA and UA.

In order to investigate stability of the films, 100 consecutive cyclic voltammograms of bare GCE, CTAB–PANI/GCE, and CTAB–PANI/AC/GCE were studied in phosphate buffer

View Article Online
DOI: 10.1039/C6RA18740D

containing mixture of DA and UA. After 100 consecutive cycles (100th cycle), the bare GCE, CTAB–PANI/GCE, and CTAB–PANI/AC/GCE have been retained 86.54, 90.43 and 95.90% of their initial catalytic response currents (1st cycle). For UA detection, 85.12, 91.80 and 94.65% of the initial response currents were retained at bare GCE, CTAB–PANI/GCE, and CTAB–PANI/AC/GCE, respectively. Apparently, the CTAB–PANI/AC/GCE is retained large percent of catalytic response currents over control electrodes which indicates its good stability during electrocatalysis. Next, the influences of different scan rates (v) to the electrocatalysis reactions of DA (**Fig. S1a**) and UA (**Fig. S1b**) are investigated. The oxidation peak currents of DA and UA are linearly increases as the scan rate increases from 20 to 200 mV s^{-1} which revealing surface confined oxidation process (**insets to Fig. S1**).

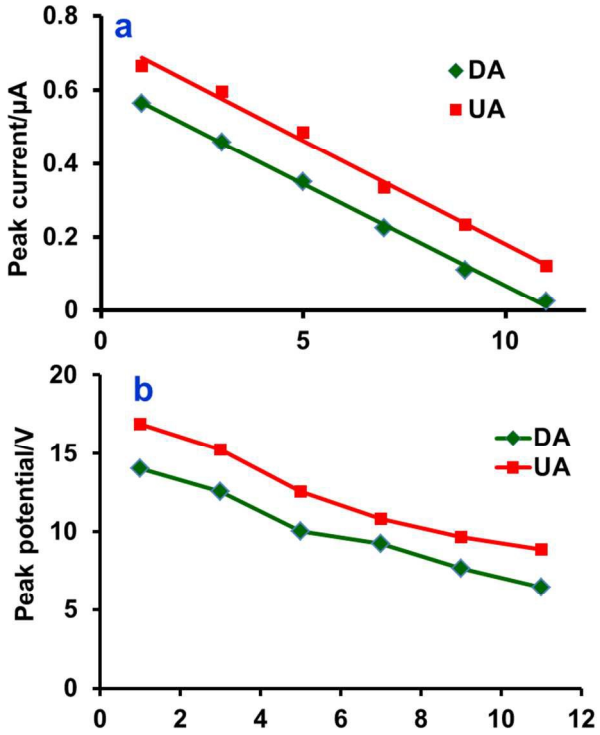

Fig. 6 (a) pH dependence of oxidation peak potentials of DA (2 mM) and UA (2 mM). (b) pH dependence of oxidation peak currents of DA (2 mM) and UA (2 mM).

The effects of electrolyte solution pH on the oxidation peak currents and peak potentials of DA and UA are examined. As shown in **fig. 6a,** the anodic peak potentials of DA and UA are negatively shifted with the increase in the pH from 1 to 11. The slopes of the plot between pH values and peak potentials exhibit good linearity (**Fig. 6b**). The slopes are – 55.3 and –56.4 (UA) pH/mV for DA and UA, respectively which indicating that equal numbers of protons and

View Article Online
DOI: 10.1039/C6RA18740D

electrons are involved in the oxidation process. The oxidation peak currents of DA and UA are predominant at low pH, while it decreases steadily when the pH changes from 1 to 11. In order to develop a sensor for biological sample, we have chosen pH 7 as the optimal working pH for our studies.

Fig. 7a presents the voltammograms obtained at CTAB–PANI/AC/GCE in presence of different concentrations of DA (**Fig. 7a**) and UA (**Fig. 7b**). As shown in figure, the modified electrode exhibited sharp oxidation peaks for each concentration of DA and UA. The oxidation peak currents are linearly increased as the concentrations of DA and UA increases. For DA, the linear range is 50–500 μM and sensitivity is 0.0517 (± 0.007) μA μM^{-1} (inset to **Fig. 7a**). For UA, the linear range is 50–500 μM and sensitivity is 0.0169 (0.009) μA μM^{-1} (inset to **Fig. 7b**).

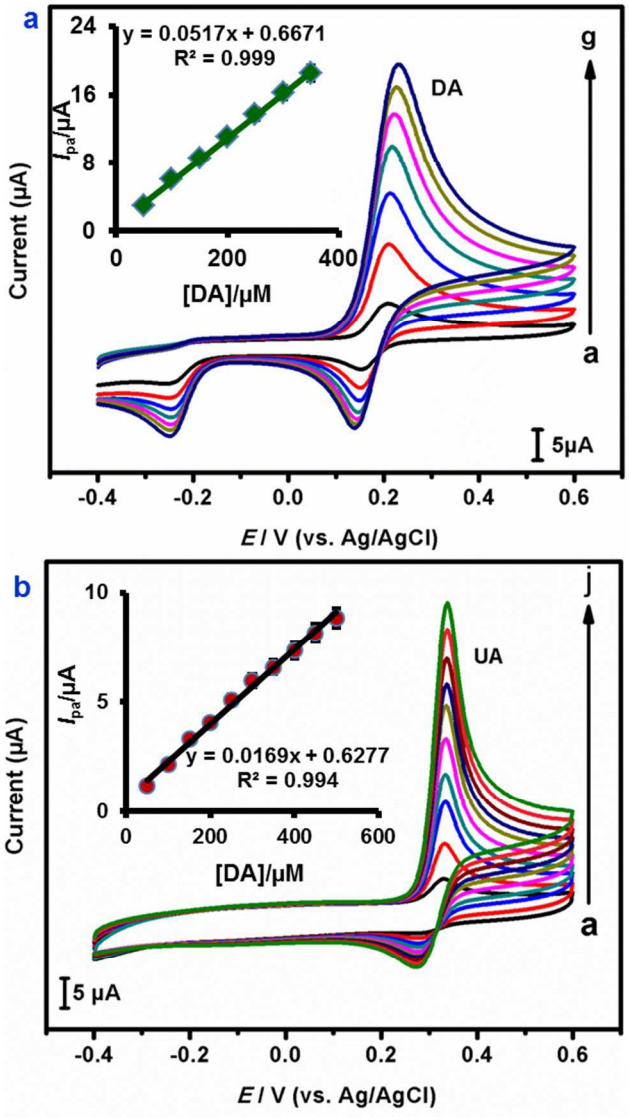

View Article Online
DOI: 10.1039/C6RA18740D

Fig. 7a CVs obtained at CTAB–PANI/AC/GCE in phosphate buffer (pH 7.0) containing DA (a=50, b=100, c=150, d= 200, e=250, f=300 and g=350 μM). b) CVs obtained at CTAB–PANI/AC/GCE in phosphate buffer containing UA (a= 50, b=100, c=150, d= 200, e=250, f=300 g=350, h=400, i=450 and j=500 μM)

3.3 Simultaneous determination of DA and UA

The main objective of the present work is to develop an electrode having higher anti-interference ability to AA. Therefore, the catalytic response of CTAB–PANI/AC/GCE towards AA is investigated through cyclic voltammetry (CV) **(Fig. S2a)** and differential pulse voltammetry (DPV) (**Fig. S2b**). The modified electrode doesn't produce any measurable signal for AA upto 2 mM in both CV and DPV analyses. Notably, the CTAB–PANI/AC composite prepared without PDS has shown selectivity upto 1 mM AA (figure not shown), while the composite prepared using PDS has shown improved selectivity upto 2 mM AA. The plausible reasons are, (1) AC surface is negatively charged which is unfavorable for negatively charged AA molecules and (2) the presence of PDS makes the electrode surface negatively charged which hinders the negatively charged AA; as a result the electrode achieved improved selectivity. Next, the electrolyte solution containing different concentrations of DA and AA in presence of fixed concentration of AA is investigated. **Fig. 8a** presents the CV curves obtained at CTAB–PANI/AC/GCE in phosphate buffer containing 2 mM AA and different concentrations of DA and UA. As presented in figure, the I_{pa} corresponding to DA and UA are linearly increased as the concentrations of DA and UA increased. The plots between peak currents and respective concentrations of DA (**Fig. 8b**) and UA (**Fig. 8c**) have shown good linearity with slopes of 2.233 and 2.883 μA/mM, respectively. Remarkably, the coexistence of AA in the mixture didn't impose any interference to the detections of DA and UA. Therefore, the CTAB–PANI/AC composite has high level of significance in the selective determinations of DA and UA. In presence of 2 mM AA co-existed solution, the modified electrode has showed linear range of 50–500 μM for DA and UA.

View Article Online
DOI: 10.1039/C6RA18740D

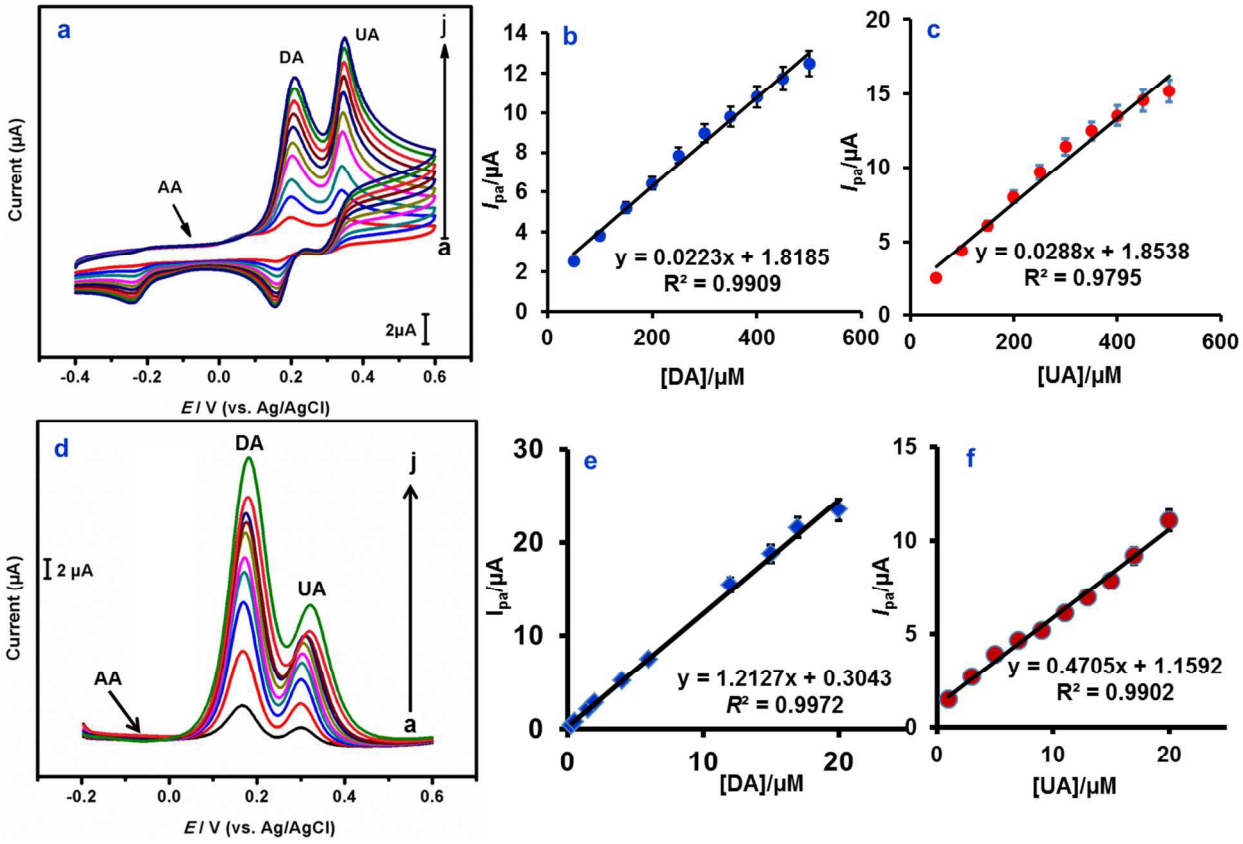

Fig. 8 (a) CVs obtained at CTAB–PANI/AC/GCE in phosphate buffer (pH 7.0) containing different concentrations of DA and UA mixture (a=50, b=100, c=150, d=200, e= 250, f=300, g=350, h=400, i=450, j=500 μM). b) I_{pa}/μA vs. [DA]/μM. c) I_{pa}/μA vs. [UA]/μM. d) DPVs of CTAB–PANI/AC/GCE in phosphate solutions (pH 7.0) containing 1.0 mM AA and mixtures of DA (0.3, 0.5, 1.5, 2.0, 4.0, 6.0, 12.0, 15.0, 17.0, 20.0 μM) and UA (1, 3, 5, 7, 9, 11, 13, 15, 17, 20 μM). e) I_{pa}/μA vs. [DA]/μM. f) I_{pa}/μA vs. [UA]/μM. The optimized parameters for DPV measurements are amplitude = 0.05 V, sampling width = 0.0167 s and pulse period = 0.5 s

In order to improve sensitivity, DPV experiments were performed. **Fig. 8d** displays the DPV curves obtained at CTAB–PANI/AC/GCE in phosphate buffer containing 2 mM AA and mixture of DA and UA. The I_{pa} of the DA and UA are linearly increases as the concentrations of DA and UA increases. The plots between concentrations of DA (**Fig. 8e**) and UA (**Fig. 8f**) with respective peak currents showed good linearity. The coexisted AA doesn't produce any interference which is consistent with the CV results. For DA and UA, the regression equations were obtained as, $[I_p]$/μA = 1.213 [DA] (μA/μM) + 0.304; R^2= 0.997 and $[I_p]$/μA = 0.471 [DA]

View Article Online
DOI: 10.1039/C6RA18740D

(μA/μM) + 1.159; R^2= 0.990, respectively. For the DA determination, the linear range is 0.3–20 μM, the sensitivity is 17.08 (± 0.09) $\mu A \mu M^{-1}$ cm^{-2} and the detection limit (LOD) is 0.06 (± 0.006) μM. For the UA determination, the linear range is 1–20 μM, the sensitivity is 6.63 (± 0.05) $\mu A \mu M^{-1}$ cm^{-2} and the LOD is 0.20 (± 0.008) μM. The LOD was calculated using the formula, LOD= 3 s_b/S (where, s_b= standard deviation of blank signal and S= sensitivity).[34] The linear range and LOD obtained for DA and UA detections at our modified electrode are comparable with previously reported modified electrodes (**Table 1**).

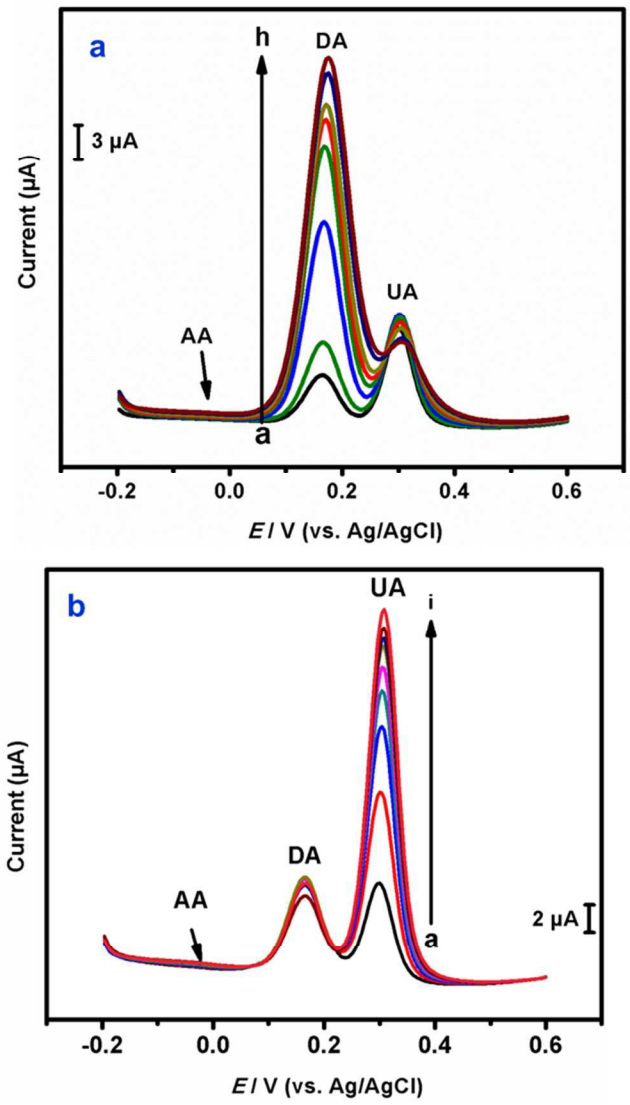

Fig. 9 (a) DPVs obtained at CTAB–PANI/AC/GCE in phosphate solutions (pH 7.0) towards different concentrations of DA: 1, 3, 10, 15, 20, 25, 30 and 35 μM containing fixed amount of (1 mM) of AA and UA. b) DPVs obtained at CTAB–PANI/AC/GCE in phosphate solutions (pH

View Article Online
DOI: 10.1039/C6RA18740D

7.0) towards different concentrations of UA: 3, 7, 10, 20, 25, 30, 35 and 40 μM containing fixed concentrations (1 mM) of AA and DA

Table 1 Comparison of the analytical performance of CTAB–PANI/AC composite with previously reported modifiers for the determinations of DA and UA

Electrodes materials	Dopamine		Uric acid		Ref
	Linear range/μM	[a]LOD/μM	Linear range/μM	LOD/μM	
poly(l–leucine)/DNA	0.1–100	0.04	0.5–100	0.2	[35]
MoS_2/[b]RGO	5–545	0.05	25–2745	0.46	[23]
PtAu hybrid film	24–384	24	20–336	21	[10]
Pd NPs/carbon nanofibers	0.5–160	0.2	2–200	0.7	[36]
Chitosan-graphene	1–24	1	2–45	2	[37]
N-doped graphene	0.5–170	0.25	0.1–20	0.045	[16]
Pt NPs/RGO	10–170	0.25	10–130	0.45	[14]
Pt NPs/polydopamine/[c]CNTs	0.25–20	0.08	0.3–13	0.12	[38]
pretreated pencil graphite	0.15–15	0.033	0.3–150	0.12	[17]
CTAB–PANI/PANI	0.3–20	0.06	1–20	0.20	This work

[a]LOD= Limit of detection; [b]RGO= Reduced graphene oxide; [c]CNTs=Carbon nanotubes

Next, selectivity of the electrode to detect DA in presence of UA and vice versa was investigated. First, DPVs were performed using the modified electrode towards different concentrations of DA containing fixed concentration of UA (1 mM) (**Fig. 9a**). As shown in figure, the electrode shows linear enhancement in peak currents for each addition of DA. The presence of UA in the supporting electrolyte wasn't produced any interference to DA oxidation. Similarly, the electrode selectively detects UA in presence of 1 mM DA and the presence of DA has no influence towards voltammetric peak of UA (**Fig. 9b**).

3.4 Stability, repeatability and reproducibility

View Article Online
DOI: 10.1039/C6RA18740D

In order to determine storage stability of the modified electrode, its electrocatalytic response towards 1 μM DA and 1 μM UA were monitored every day. The modified electrode was stored in phosphate buffer (pH 7) at 4°C when not in use. During 15 days of its storage period, 92.16% and 91.05% of the initial oxidation peak currents were retained for DA and UA, respectively. Next, repeatability of the electrode was evaluated by performing five repeatitive measurements using independently prepared modified electrodes in phosphate buffer containing mixture of DA and UA. The electrode has shown satisfactory repeatability with RSD of 4.12% and 3.87% for DA and UA detections, respectively. Similarly, reproducibility of the electrode was evaluated for five independent measurments performed using five different modified electrodes in phosphate buffer containing mixture of DA and UA. The electrode delivers good reproducibility for the determinations of DA and UA with RSD of 3.68 and 3.80%, respectively.

Table 2 Determination of DA and UA in real samples using CTAB–PANI/AC/GCE

Real Samples	DA				UA			
	Added/μM	Found/μM	Recovery/%	*RSD/%	Added/μM	Found/μM	Recovery/%	*RSD/%
Human serum	10	10.45	104.5	3.51	5	4.78	95.6	2.54
	20	19.34	96.7	3.95	10	9.62	96.2	3.95
Urine sample	10	9.86	98.6	3.82	5	4.82	96.4	4.20
	20	19.24	96.2	3.40	10	9.81	98.1	3.18
Rat brain	10	9.61	96.1	4.22	–	–	–	–
	20	19.18	95.9	4.58	–	–	–	–
Dopamine Injection	10	9.74	97.4	3.61	–	–	–	–
	20	19.37	96.85	4.08	–	–	–	–

* Related standard deviation (RSD) of 3 independent experiments

3.5 Real sample analysis

The real-time application of the modified electrode was demonstrated in rat brain, dopamine injection, human serum and urine samples. The sampling procedure is given in section 2. 3. Known concentrations of DA and UA (mixtures) were spiked into these solutions and DPV

View Article Online
DOI: 10.1039/C6RA18740D

experiments were carried out. The dopamine injection sample was directly used without any dilution. For each real sample, the CTAB–PANI/AC/GCE presents quick and sensitive DPV signals which were consistent with the results obtained in lab samples analyses. The added, found and recovery values are calculated and given as **Table 2**. It can be seen from the table that the modified electrode able to detect DA and UA with satisfactory range of recoveries (95.6–104.5%). Thus, the CTAB–PANI/AC composite has good practicality and it can be used for the real-time determinations of DA and UA.

4. Conclusions

In summary, a sensitive and highly selective electrochemical DA and UA detection platform was developed using CTAB–PANI/AC composite. The successful formation of the composite was confirmed by SEM, EIS and electrochemical methods. The CTAB–PANI/AC composite film modified electrode exhibited excellent electrocatalytic ability to determine DA and UA. The electrode is highly selective to detect DA and UA even in presence of high concentrations of AA (upto 2 mM). The DPV based sensing platform was developed which shown excellent analytical parameters for both DA and UA with detection limits of 0.06 (± 0.006) μM and 0.20 (± 0.008) μM. Also, the modified electrode has satisfactory stability, repeatability and reproducibility. The composite has promising practical applicability in rat brain, dopamine injection, and human serum and urine samples.

Acknowledgement

The authors extend their appreciation to the International Scientific Partnership Program ISPP at King Saud University for funding this research work through ISPP#6. This work was supported by the Ministry of Science and Technology (MOST), Taiwan (ROC).

References

1. V. Vasantha and S.-M. Chen, *Journal of Electroanalytical Chemistry*, 2006, **592**, 77-87.
2. H. Sun, J. Chao, X. Zuo, S. Su, X. Liu, L. Yuwen, C. Fan and L. Wang, *RSC Advances*, 2014, **4**, 27625-27629.
3. R. A. Wise, *Nature Reviews Neuroscience*, 2004, **5**, 483-494.
4. Y. Wang, Y. Li, L. Tang, J. Lu and J. Li, *Electrochemistry Communications*, 2009, **11**, 889-892.
5. M. Lin, *RSC Advances*, 2015, **5**, 9848-9851.
6. J. Du, R. Yue, F. Ren, Z. Yao, F. Jiang, P. Yang and Y. Du, *Gold Bulletin*, 2013, **46**, 137-144.

View Article Online
DOI: 10.1039/C6RA18740D

7. R. Devasenathipathy, V. Mani, S.-M. Chen, B. Viswanath, V. Vasantha and M. Govindasamy, *RSC Advances*, 2014, **4**, 55900-55907.
8. B. Kong, A. Zhu, Y. Luo, Y. Tian, Y. Yu and G. Shi, *Angewandte Chemie*, 2011, **123**, 1877-1880.
9. C. Yang, E. Trikantzopoulos, M. D. Nguyen, C. B. Jacobs, Y. Wang, M. Mahjouri-Samani, I. N. Ivanov and B. J. Venton, *ACS Sensors*, 2016, **1**, 508-515.
10. S. Thiagarajan and S.-M. Chen, *Talanta*, 2007, **74**, 212-222.
11. H. Y. Yue, S. Huang, J. Chang, C. Heo, F. Yao, S. Adhikari, F. Gunes, L. C. Liu, T. H. Lee and E. S. Oh, *ACS nano*, 2014, **8**, 1639-1646.
12. Z. Wang, J. Liu, Q. Liang, Y. Wang and G. Luo, *Analyst*, 2002, **127**, 653-658.
13. M. Liu, Q. Chen, C. Lai, Y. Zhang, J. Deng, H. Li and S. Yao, *Biosensors and Bioelectronics*, 2013, **48**, 75-81.
14. T.-Q. Xu, Q.-L. Zhang, J.-N. Zheng, Z.-Y. Lv, J. Wei, A.-J. Wang and J.-J. Feng, *Electrochimica Acta*, 2014, **115**, 109-115.
15. J. Sun, L. Li, X. Zhang, D. Liu, S. Lv, D. Zhu, T. Wu and T. You, *RSC Advances*, 2015, **5**, 11925-11932.
16. Z.-H. Sheng, X.-Q. Zheng, J.-Y. Xu, W.-J. Bao, F.-B. Wang and X.-H. Xia, *Biosensors and Bioelectronics*, 2012, **34**, 125-131.
17. E. Alipour, M. R. Majidi, A. Saadatirad, S. mahdi Golabi and A. M. Alizadeh, *Electrochimica Acta*, 2013, **91**, 36-42.
18. L.-N. Wu, Y.-L. Tan, L. Wang, S.-N. Sun, Z.-Y. Qu, J.-M. Zhang and Y.-J. Fan, *Microchimica Acta*, 2015, **182**, 1361-1369.
19. Y. Wu, Z. Dou, Y. Liu, G. Lv, T. Pu and X. He, *RSC Advances*, 2013, **3**, 12726-12734.
20. C. R. Raj, T. Okajima and T. Ohsaka, *Journal of Electroanalytical Chemistry*, 2003, **543**, 127-133.
21. S. Yang, G. Li, Y. Yin, R. Yang, J. Li and L. Qu, *Journal of Electroanalytical Chemistry*, 2013, **703**, 45-51.
22. S. Thirumalairajan, K. Girija, V. R. Mastelaro, V. Ganesh and N. Ponpandian, *RSC Advances*, 2014, **4**, 25957-25962.
23. L. Xing and Z. Ma, *Microchimica Acta*, 2016, **183**, 257-263.
24. A. Liu, I. Honma and H. Zhou, *Biosensors and Bioelectronics*, 2007, **23**, 74-80.
25. S. Khalili, B. Khoshandam and M. Jahanshahi, *RSC Advances*, 2016, **6**, 35692-35704.
26. M. R. Karim, C. J. Lee and M. S. Lee, *Journal of applied polymer science*, 2007, **103**, 1973-1977.
27. D. S. Patil, S. A. Pawar, R. S. Devan, Y. R. Ma, W. R. Bae, J. H. Kim and P. S. Patil, *Materials Letters*, 2014, **117**, 248-251.
28. M. Oh and S. Kim, *Journal of nanoscience and nanotechnology*, 2012, **12**, 519-524.
29. Z. Jin, X. Ren, C. Qin, B. Li, S. Quan and X. Bai, *Pigment & Resin Technology*, 2011, **40**, 235-239.
30. S. Xing, Y. Chu, X. Sui and Z. Wu, *Journal of materials science*, 2005, **40**, 215-218.
31. V. Mani, M. Govindasamy, S.-M. Chen, R. Karthik and S.-T. Huang, *Microchimica Acta*, 2016, 1-9.
32. W. Naqash and K. Majid, *Materials Research*, 2015, **18**, 1121-1127.
33. D. Liu, X. Wang, J. Deng, C. Zhou, J. Guo and P. Liu, *Nanomaterials*, 2015, **5**, 1034-1047.
34. V. Mani, A. P. Periasamy and S.-M. Chen, *Electrochemistry Communications*, 2012, **17**, 75-78.
35. X. Zheng, Y. Guo, J. Zheng, X. Zhou, Q. Li and R. Lin, *Sensors and Actuators B: Chemical*, 2015, **213**, 188-194.
36. J. Huang, Y. Liu, H. Hou and T. You, *Biosensors and Bioelectronics*, 2008, **24**, 632-637.
37. D. Han, T. Han, C. Shan, A. Ivaska and L. Niu, *Electroanalysis*, 2010, **22**, 2001-2008.
38. M. Lin, H. Huang, Y. Liu, C. Liang, S. Fei, X. Chen and C. Ni, *Nanotechnology*, 2013, **24**, 065501.

View Article Online
DOI: 10.1039/C6RA18740D

Table of content

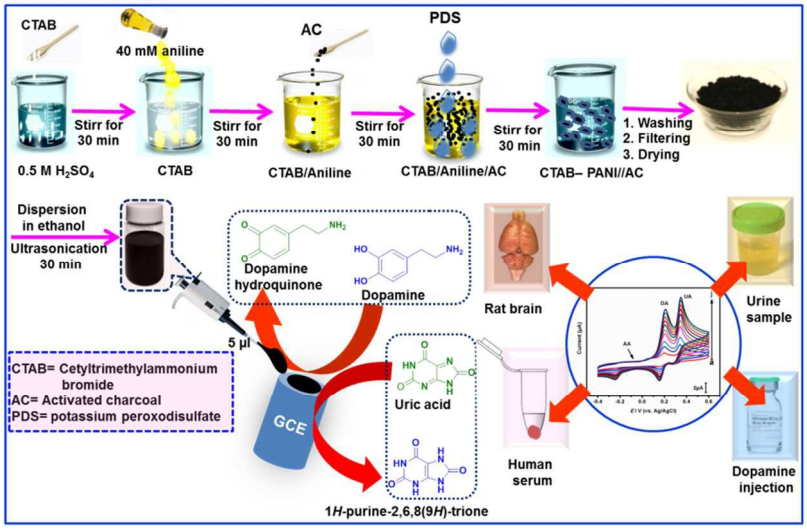

Simultaneous determination of dopamine and uric acid have been described using CTAB–PANI/ activated charcoal composite with detection limits of 0.06 µM and 0.20 µM, respectively. The composite does not produced any signal for ascorbic acid. Practicality is demonstrated in rat brain, dopamine injection, and human serum and urine samples